East European Journal of Physics. **4.** 286-293 (2023)
DOI:10.26565/2312-4334-2023-4-36 ISSN 2312-4334

ENHANCED HEAT TRANSFER ANALYSIS ON MHD HYBRID NANOFLUID FLOW OVER A POROUS STRETCHING SURFACE: AN APPLICATION TO AEROSPACE FEATURES

R. Chandra Sekhar Reddy, Gunisetty Ramasekhar*
Department of Mathematics, Rajeev Gandhi Memorial College of Engineering and Technology (Autonomous), Nandyal 518501, Andhra Pradesh, India
**Corresponding Author e-mail: gunisettyrama@gmail.com*
Received October 1, 2023; revised October 24, 2023; accepted November 6, 2023

The advancement of aircraft technology has presented manufacturers with new criteria and problems for the functioning of their devices. It is essential that, in order to guarantee the secure operation of aerospace machinery, the failure mechanisms be identified, and the operational durability of critical structural components be improved as quickly as possible. New aviation materials have been developed in the modern years. In an aviation engine, engine oil lubricates, cools, washes, maintains against rust, decreases sound, and accelerates. The most important is lubrication. All mechanical components would burn out if not maintained. The aim of this work is to minimize costs by extending the operational life of aircraft components (mechanical and motor parts) and enhancing fuel mileage and flying distance. Based on the importance of the inspiration on magnetohydrodynamic Aluminum Oxide-Cobalt hybrid nanofluid flow over a stretching surface in the existence of a porous medium, thermal radiation is investigated. In this model, we used Engine oil mixed with Aluminum Oxide and Cobalt nanoparticles. By using the suitable self-similarity variables, the PDE is transformed into ODEs. After that, the dimensionless equations are solved by using the Maple built-in BVP Midrich scheme. Graphs and tables explain how the operational factors affect fluid flow efficiency. Compared to nanofluids, hybrid nanofluids have a better heat transfer rate.
Keywords: *BVP Midrich scheme; MHD; Thermal radiation; Porous medium; Hybrid nanofluid*
PACS: 44.05.+e, 44.30.+v, 44.40.+a, 47.10.ad

INTRODUCTION

The movement of heat from one location to another is a critical step in the process of either central heating or central cooling an item. The considerable heat that is generated must be reduced to a reasonable level or dissipated in order for a device or system to function at its highest possible standard. In order to minimize heat on equipment such as processors and in a number of sectors such as automotive and technology, fluid refrigerants have historically been employed [1]. However, traditional liquid refrigerants have a weak heat transfer [2]. Because of this, there is a greater potential for creativity and technological improvement in the field of cooling. The use of nanofluid, which is a fluid that includes nanoparticles, is one of the methods that has been established to improve the efficiency of heat transfer in liquid refrigeration systems [3], [4]. The issue with fluid containing dispersed nano meter particles is coagulation, deposition, and flow line blockage. The aforementioned issues might be partly addressed by employing nanomaterials embedded as micro particles. Nanofluids are extensively employed in semiconductors, automotive, power, and universal healthcare industries, among others, owing to their appealing high - temperature, visual, and electromagnetic characteristics [5]–[7].

An innovative approach of mixing two or three kinds of metallic nanoparticles within the base fluid to boost thermal performance has been developed. Hybrid nanofluid mixes metallic nanoparticles in base fluid. Using hybrid nanofluids to chill or warm machines enhances heat transmission [8], [9]. Many researchers have studied nanoparticle combinations in base fluids to create a refrigerant with superior thermal conductivity. Temperature distribution and heat capacity of hybrid nanofluid are influenced by particle diameter, volume fraction, thermal efficiency, and viscosity [10]. Nanofluid improves material impact energy and is an excellent refrigerant. Among the several metals that are used in the study of nanofluids, Alumina, due to its chemical stability and increased mechanical power, is often employed in the investigation of hybrid nanofluids. Other types of cobalt alloys are put to use in devices like jet turbines, which need high hardness. Electroplating is sometimes performed using cobalt metal because of its excellent standards, high level of hardness, and excellent corrosion resistance.

Magnetohydrodynamics, reduced as (MHD), is the study of fluids that have associated electric currents and are placed in a magnetic field. Magneto-fluid dynamics is the term that describes this process. Examples of magneto-fluids include plasmas, ions, seawater, and liquid crystals. Hannes Alfvin was given the Nobel Prize in Physics that year, which was granted in 1970 for his ground-breaking work in the field of MHD. The magneto-nanofluid combines the characteristics of magnets and liquids into a single substance. The magnetic impacts not only radicalize the particles in the liquid system but also create a modification in heat transfer. Additionally, the magnetic effects cause the absorption to be reconstructed. Because they contain more viscous body cells than non-malignant nanoparticles and because the cells improve blood circulation, magnetic nanoparticles are used in the biomedical industry [11]–[13]. MHD has received a lot of attention in astronomy, healthcare, optical transplants, metal processing, geophysical disciplines, and petrochemical engineering [14].

Cite as: R.C.S. Reddy, G. Ramasekhar, East Eur. J. Phys. 4, 286 (2023), https://doi.org/10.26565/2312-4334-2023-4-36
© R.C.S. Reddy, G. Ramasekhar, 2023; CC BY 4.0 license

Engine oil is used in power turbines, motor engines, and machines, including cars. Contact between shifting gears in mechanical systems reduces efficiency by heating dynamic energy. Oil's primary function is to reduce contact between moving components. The engine oil may cool contacting parts, however. Heat transfer and thickness of engine oil are important for mechanical cooling and lubrication. The viscosity influences pumping force and oil circulation. This study also considers cobalt and aluminium oxide. Cobalt-based fantastic alloys are recycled in jet machines, with military warrior planes, owing to their immovability at high temperatures. Al_2O_3 is a great ceramic oxide by a varied range of uses, with aerospace manufacturing, and additional high-modernization arenas [15], [16].

MOTIVATION OF THE PROPOSED MODEL

According to the current literature, no research has been done to analyse the concept of magnetohydrodynamic (MHD) over a stretching surface with the presence of porous medium and linear thermal radiation. The equations that are created are in the form of PDE. To convert the PDE into ODEs, a self-similarity transformation is used. After applying transformations, for the graphical purpose, we have used the Maple built in BVP Midrich scheme. In this study we employ the Engine oil as a base fluid and Aluminium Oxide - Cobalt are hybrid nanofluids. This model plays an essential role in aerospace machinery, nuclear reactor cooling, and vehicles. In the results and discussion section, graphs for different physical significance are given. As a result, the researchers are confident that the new study is unique, will have a considerable influence in the domains of engineering and mathematics, and has the opportunity to encourage new investigators.

MATHEMATICAL FORMULATION

In addition to a stretched surface, a two-dimensional heat transfer representation is examined in a mixed-heat-dispersal (MHD) aluminium oxide–cobalt hybrid nanofluid. Within the framework of the energy and temperature equation, thermal radiation is taken into account. As can be seen in Table 1, two distinct kinds of nanoparticles, namely Al_2O_3 and cobalt, are suspended in the base fluid engine oil. The velocity components u and v are measured along the x-axis and the y-axis, respectively; the velocity is written as $u_w = ax$. Furthermore, the temperature of the sheet as well as the temperature of the free stream is represented by the symbols T_w, T_∞, which is demonstrated in Figure 1, respectively.

Table 1. Thermophysical properties of Engine oil, Al_2O_3-Cobalt hybrid nanofluid [19].

Property	Engine oil	Al_2O_3	Cobalt
Density $\rho\,(kgm^{-3})$	863	3970	8900
Specific heat $C_p\,(Jkg^{-1}K^{-1})$	2048	765	420
Heat conductivity $k_f\,(Wm^{-1}K^{-1})$	0.1404	40	100
Electrical conductivity $\sigma\,(\Omega m)^{-1}$	55×10^{-6}	1×10^{-10}	1.602×10^{7}
Pr	6450		

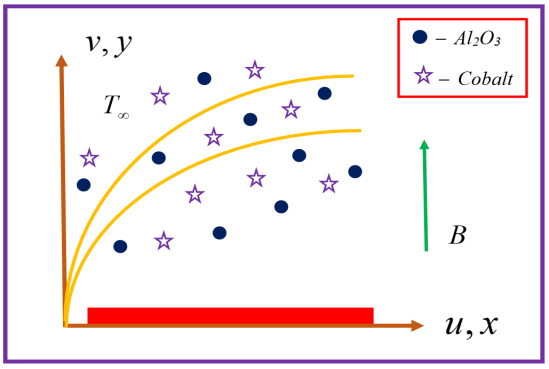

Figure 1. Geometry of the problem.

The governing flow equations are constructed as [17], [18]

$$\frac{\partial u}{\partial x}+\frac{\partial u}{\partial y}=0, \tag{1}$$

$$u\frac{\partial u}{\partial x}+v\frac{\partial u}{\partial y}=\frac{\mu_{hnf}}{\rho_{hnf}}\left(\frac{\partial^2 u}{\partial y^2}\right)-\frac{\mu_{hnf}}{\rho_{hnf}}\frac{u}{K^*}-\frac{\sigma_{hnf}}{\rho_{hnf}}\left(B^2u\right), \tag{2}$$

$$u\frac{\partial T}{\partial x}+v\frac{\partial T}{\partial y}=\frac{k_{hnf}}{\left(\rho c_p\right)_{hnf}}\left(\frac{\partial^2 T}{\partial y^2}\right)-\frac{1}{\left(\rho c_p\right)_{hnf}}\left(\frac{\partial q_r}{\partial y}\right)+\frac{\sigma_{hnf}B^2}{\left(\rho c_p\right)_{hnf}}u^2. \tag{3}$$

By Rosseland approach, we have

$$q_r = -\frac{4\sigma^*}{3k^*}\frac{\partial T^4}{\partial y}. \tag{4}$$

By applying the Taylor's series expansion of T^4 about T_∞ and neglecting terms having higher order, we obtain

$$T^4 = 4T_\infty{}^3 T - 3T_\infty{}^4. \tag{5}$$

Putting Eq. (5) in Eq. (3), we get

$$u\frac{\partial T}{\partial x} + v\frac{\partial T}{\partial y} = \frac{k_{hnf}}{\left(\rho c_p\right)_{hnf}}\left(\frac{\partial^2 T}{\partial y^2}\right) - \frac{1}{\left(\rho c_p\right)_{hnf}}\frac{16T_\infty^3}{3k^*}\frac{\partial^2 T}{\partial y^2} + \frac{\sigma_{hnf}B^2}{\left(\rho c_p\right)_{hnf}}u^2. \tag{6}$$

The corresponding boundary conditions are:

$$\begin{aligned} &u = u_w(x) = ax, v = 0, k_{hnf}\frac{\partial T}{\partial y} = h_f\left(T_f - T\right), && at\ y = 0 \\ &u \to 0, T \to T_\infty && as\ y \to \infty. \end{aligned} \tag{7}$$

The following suitable self-similarity transformations are defined as:

$$u = axf'(\eta), v = -\sqrt{a\upsilon_f}\,f(\eta), \theta(\eta) = \frac{T - T_\infty}{T_f - T_\infty}, \eta = y\sqrt{\frac{a}{\upsilon_f}}. \tag{8}$$

Thermophysical properties of *hnf* are

$$K_1 = \frac{\mu_{hnf}}{\mu_f}, K_2 = \frac{\rho_{hnf}}{\rho_f}, K_3 = \frac{(\rho c_p)_{hnf}}{(\rho c_p)_f}, K_4 = \frac{k_{hnf}}{k_f}, K_5 = \frac{\sigma_{hnf}}{\sigma_f}.$$

$$\left.\begin{aligned} K_1 &= \frac{1}{(1-\phi_1)^{2.5}(1-\phi_2)^{2.5}}, \\ K_2 &= \left\{(1-\phi_2)\left[(1-\phi_1) + \phi_1\left(\frac{\rho_{s_1}}{\rho_f}\right)\right] + \phi_2\frac{\rho_{s_2}}{\rho_f}\right\}, \\ K_3 &= (1-\phi_2)\left[(1-\phi_1) + \phi_1\left(\frac{(\rho c_p)_{s_1}}{(\rho c_p)_f}\right)\right] + \phi_2\frac{(\rho c_p)_{s_2}}{(\rho c_p)_f}, \\ K_4 &= \frac{k_{s_1} + 2k_{bf} - 2\phi_2(k_{bf} - k_{s_2})}{k_{s_2} + 2k_{bf} + \phi_2(k_{bf} - k_{s_2})} \times \frac{k_{s_1} + 2k_f - 2\phi_1(k_f - k_{s_1})}{k_{s_1} + 2k_f + \phi_1(k_f - k_{s_1})}, \\ K_5 &= \frac{\sigma_{s_2} + 2\sigma_{nf} - 2\phi_2(\sigma_{nf} - \sigma_{s_2})}{\sigma_{s_2} + 2\sigma_{nf} + \phi_2(\sigma_{nf} - \sigma_{s_2})} \times \frac{\sigma_{s_1} + 2\sigma_f - 2\phi_1(\sigma_f - \sigma_{s_1})}{\sigma_{s_1} + 2\sigma_f + \phi_1(\sigma_f - \sigma_{s_1})}. \end{aligned}\right\} \tag{9}$$

In order to create the following dimensionless ODEs, Eqs. (2) and (6) are transformed using the ideal technique indicated in Eq (8).

$$\frac{K_1}{K_2}f''' + K_2\left(ff'' - (f')^2\right) - \frac{K_1}{K_2}Kf' - \frac{K_5}{K_2}Mf' = 0, \tag{10}$$

$$\theta''\left(K_4 + \frac{4}{3}Rd\right) + K_3 Prf\theta' + \frac{K_5}{K_3}MEc(f')^2 = 0. \tag{11}$$

The boundaries of the change are described as:

$$\begin{aligned} &f(0) = 0, f'(0) = 1, K_4\theta'(0) = -Bi\left(1 - \theta(0)\right) \\ &f'(\infty) = 0, \theta'(\infty) = 0. \end{aligned} \tag{12}$$

Note that $M=\frac{\sigma_f B^2}{\rho_f a}$ is the magnetic field parameter, $Pr=\frac{\mu_f\left(c_p\right)_f}{k_f}$ is the Prandtl number, $Rd=\frac{4\sigma^* T_\infty^3}{k^* k_f}$ is the Radiation parameter, $Bi=\frac{h_f}{k_f}\sqrt{\frac{\upsilon_f}{a}}$ is the Biot number, $Ec=\frac{a^2x^2}{c_p\left(T_f-T_\infty\right)}$ is the Eckert number, and $K=\frac{\upsilon_f}{aK^*}$ is the porosity parameter.

The dimensional form of skin-friction coefficient, and Nusselt numbers are expressed as

$$C_f=\frac{\tau_w}{\rho_f u_w^2} \tag{13}$$

Where shear stress τ_w is $\tau_w=\mu_{hnf}\left.\frac{\partial u}{\partial y}\right|_{y=0}$

$$Nu=\frac{xq_w}{k_f\left(T_w-T_\infty\right)} \tag{14}$$

Where heat flux q_w is $q_w=-k_{hnf}\left.\frac{\partial T}{\partial y}\right|_{y=0}$

The Non-dimensional form of Eqs. (13–14) converts are

$$Re_r^{1/2}C_f=Cf=K_1 f''(0), \tag{15}$$

$$Re_r^{-1/2}Nu_r=Nu=-K_4\theta'(0). \tag{16}$$

Where Re_r is the local Reynolds number.

SOLUTION METHODOLOGY

The nature of the ODE system (10–11) with BCs (12) is extremely nonlinear in its characteristics. For the purpose of dealing with these equations, we adopt a computational approach known as the BVP Midrich method. Using Maple, we are able to solve the control problem. The midway method's standard operating procedure is laid out in detail below. The following is a demonstration of the overall algorithm for the technique of midpoint collocation

$$\overline{Z'}(x)=F\left(x,\overline{Z}(x)\right),\quad \overline{Z}(x_0)=\overline{Z_0}, \tag{17}$$

In the explicit midpoint approach, also known as the Modified Euler method, the formula looks like this

$$\overline{Z_{n+1}}=\overline{Z_n}+hF\left(x_n+\frac{h}{2},\overline{Z_n}+\frac{h}{2}F\left(x_n,\overline{Z_n}\right)\right), \tag{18}$$

The above equation *h* represents the step size and $x_n=(x_0+nh)$.

The strategy that takes into account the implicit midpoint may be described as

$$\overline{Z_{n+1}}=\overline{Z_n}+hF\left(x_n+\frac{h}{2},\ \overline{Z_n}+\frac{1}{2}\left(\overline{Z_n},\ \overline{Z_{n+1}}\right)\right),\qquad n=0,1,2,... \tag{19}$$

At each step size, the technique for locating the midpoint has a local error of order $O(h^3)$ whereas the global error is of order $O(h^2)$. When dealing with algorithms that are more quantifiable demanding, the algorithm-error decreases at a quicker rate as $h\to 0$ progresses, and the result gets more dependable.

RESULTS AND DISCUSSION

The non-dimensional controlling flow model (10) – (11), which are subject to the boundary conditions (12), may be solved numerically with the assistance of Maple built in BVP Midrich scheme. We took the values of non-dimensional parameters and evaluated. The precise solutions are obtained from Table 2, which demonstrations the variations in skin friction coefficient. The findings of both investigations were determined to be fairly accurate. Figure 2 shows that the numerical process for BVP Midrich technique.

Table 2. Comparison table for various Prandtl numbers of the current study.

Pr	Ali et al. [17]	Present results
0.7	0.4560	0.45532
2.0	0.9113	0.91032

The effect of M on the velocity sketch is seen in Figure 3. It can be seen that the velocity profile has a decreasing trend for higher M values, which indicates that the value of M is increasing. Physically speaking, an increase in M causes a Lorentz force to be produced, which retards the movement of the liquid. As a consequence of the fact that the Lorentz force is antagonistic to the motion of fluids, the flow velocity decreases as a consequence of the increased resistance, which in turn leads to a drop in the velocity field. When increases the K values improves the velocity outline, which is demonstrated in Figure 4, physically by raising the K values, a porous substance becomes more difficult to flow across, retarding the flow of fluids. As a direct and immediate consequence of this, the dimension of the outermost boundary layer is decreased.

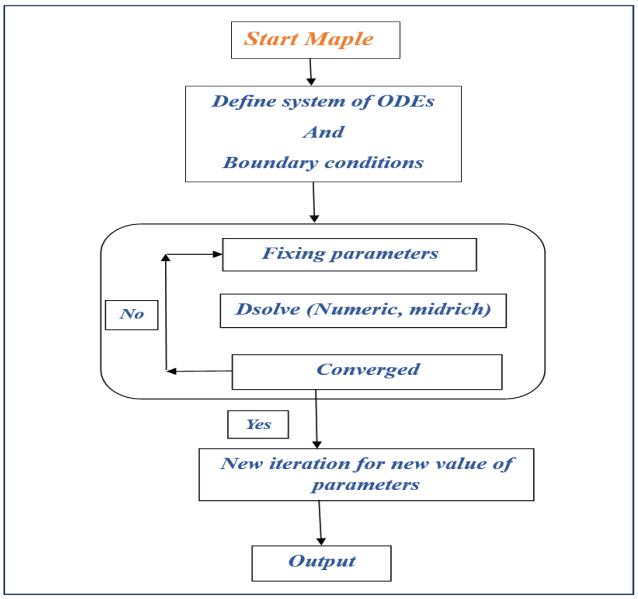

Figure 2. A flow chart pictogram of BVP Midrich technique.

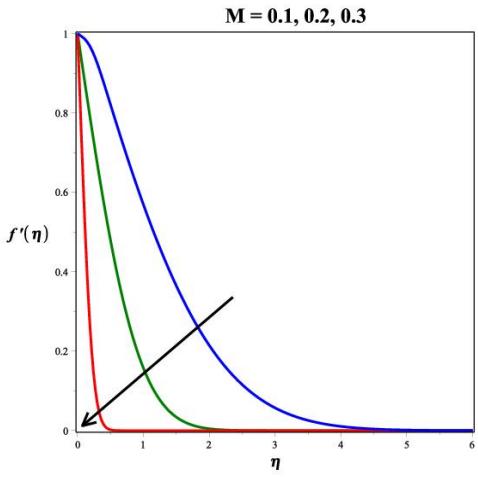

Figure 3. Pictogram of M on $f'(\eta)$.

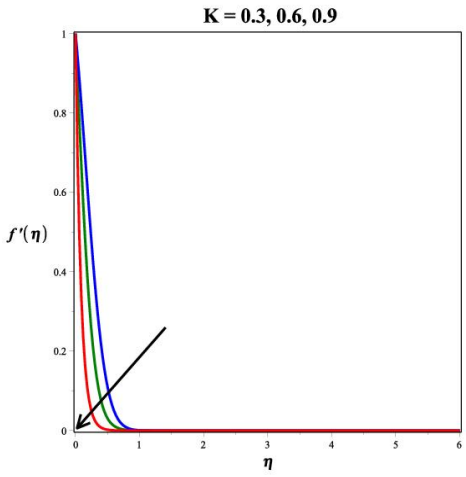

Figure. 4. Pictogram of K on $f'(\eta)$.

The influence of magnetic field on temperature profile is seen in Figure 5. It states that growing the M parameter increased the energy outline. This enhancement is due to the fact that the addition of a M into an electrically conducting material produces a resistive Lorentz force. This kind of force has the ability to raise the fluids temperature. So, this reason the temperature profile enhances. Figure 6 shows the radiation parameter temperature profile features. Physically, thermal radiation is the radiant energy released by all generators above zero. Electromagnetic radiation from heated surfaces rotates atoms in matter, generating kinetic energy. The graph demonstrates how increasing radiation enhances heat transmission. When Rd is raised, more heat is transmitted into the liquid, strengthening the thermal barrier. Since the mean absorption coefficient drops as radiation growths, temperature also increases. The effect of Eckert number on energy profile is seen in Figure 7. It states that growing the Ec values are increased the temperature outline. Physically, Ec generates the frictional forces which cause to increase the fluid temperature. The influence of Pr on energy profile is seen in Figure 8. It states that increasing the Pr values are enhanced the temperature outline. The thermal dissipation of the liquid essentially reduces, resulting in a decrease in temperature outline.

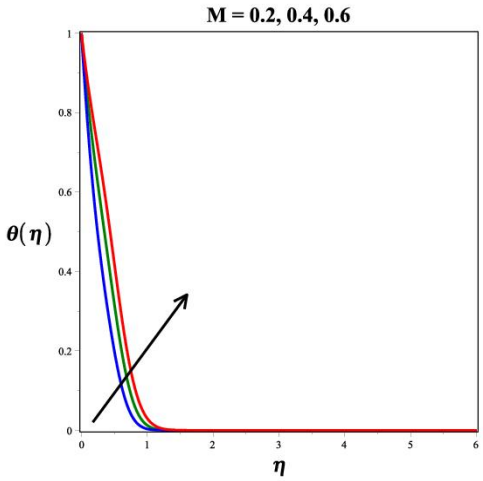

Figure. 5. Pictogram of M on $\theta(\eta)$.

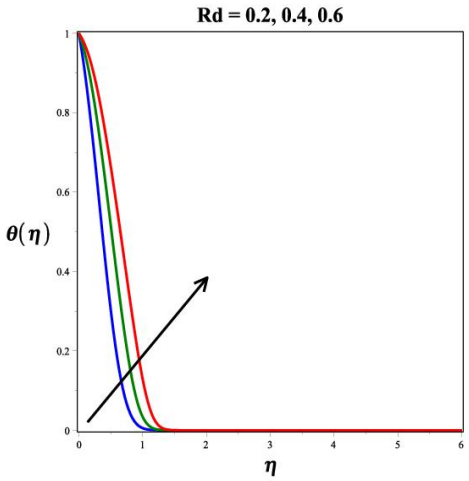

Figure. 6. Pictogram of Rd on $\theta(\eta)$.

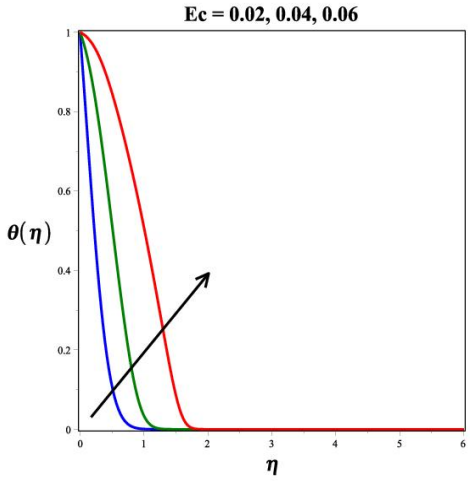

Figure. 7. Pictogram of Ec on $\theta(\eta)$.

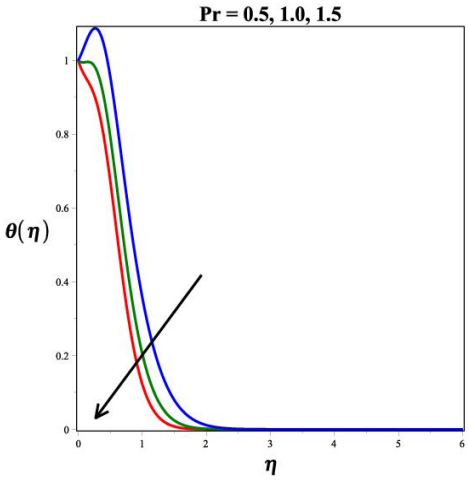

Figure. 8. Pictogram of Pr on $\theta(\eta)$.

Figure 9 and 11 displays the influence of the K and M on the Cf. It shows that the skin friction factor is decreasing for the greater values of K and M, while the reverse nature we observed on Figure 11. Figure 10 and 12 demonstrate the inspiration of the Rd and magnetic field on the Nu profile. It shows that the Nu is enhancing in all cases of the greater values of Rd and magnetic field. Figures 13 and 14 exhibit magnetic parameter for various values of $M = 0.5, 1.0$ influences on streamlines plots. Magnetic parameter strength draws electrical conductivity molecules more towards to the main stream.

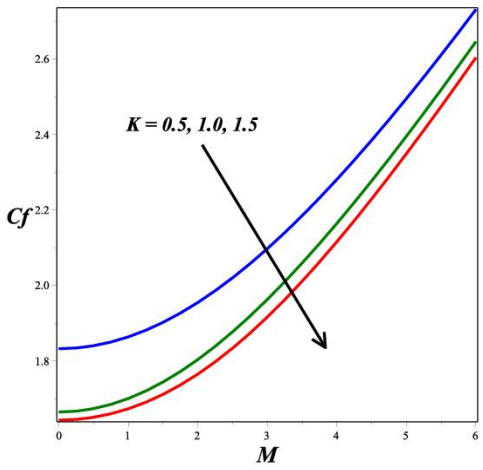

Figure 9. Sway of K *and* M on Cf.

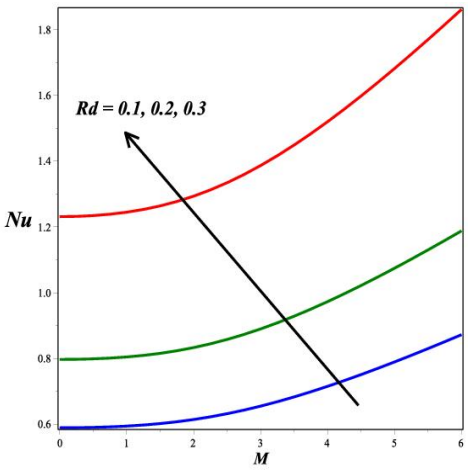

Figure 10. Sway of Rd *and* M on Nu.

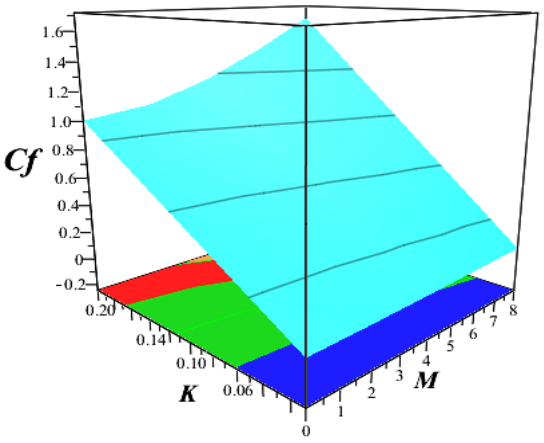

Figure 11. Sway of K *and* M on Cf .

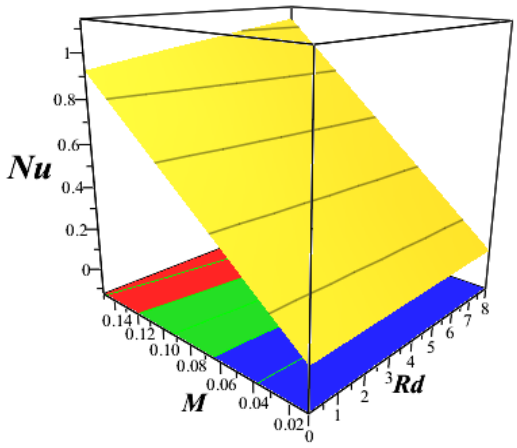

Figure 12. Sway of M *and* Rd on Nu .

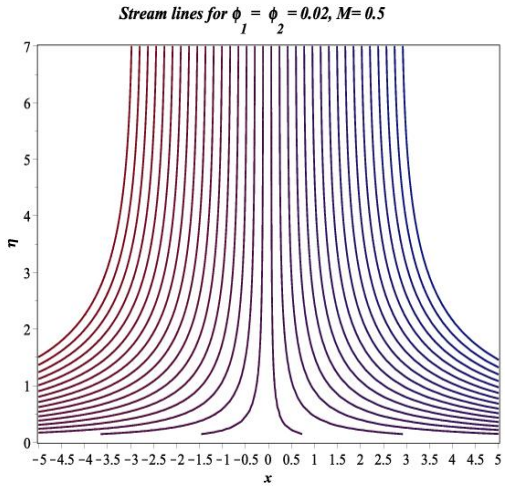

Figure 13. Stream lines for $M = 0.5$.

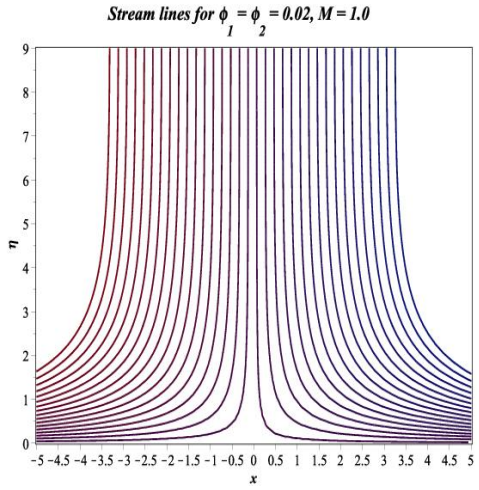

Figure 14. Stream lines for $M = 1.0$.

CONCLUSIONS

The current research study explored the numerical solution for MHD of Al_2O_3-Cobalt/Engine oil hybrid nanofluid over a Stretching surface. The Numerical method (BVP Midrich scheme) was used to solve the issue of velocity, temperature and the outcome was truly solution to the model. The results are presented in a variety of graphical formats, including a two-dimensional plot, 3D surface plots, and streamlines.

The research produced a number of interesting findings, which are listed below:

- Velocity profile decreases for the increasing values of the magnetic field and porosity parameter values.
- The temperature profile improved with an improvement in the radiation parameter.
- The skin friction factor slowly increased for the larger values of the porous parameter.
- The *Nu* profile enhanced, for the increasing values of the *M* and *Rd*.
- Streamlines have an oscillating character, which is necessary for magnifying the magnetic field parameter.

ORCID

Gunisetty Ramasekhar, https://orcid.org/0000-0002-3256-3145

REFERENCES

[1] M. Sheikholeslami, *Application of control volume based finite element method (CVFEM) for nanofluid flow and heat transfer*, (Elsevier Science, 2018).

[2] S. Das, S.U. S. Choi, and H.E. Patel, "Heat transfer in nanofluids - a review," Heat Transfer Engineering, **27**(10), 3–19 (2007). https://doi.org/10.1080/01457630600904593

[3] B.A. Bhanvase, D.P. Barai, S.H. Sonawane, N. Kumar, and S.S. Sonawane, "Intensified Heat Transfer Rate With the Use of Nanofluids," in: *Intensified heat transfer rate with the use of nanofluids*, (Elsevier, 2018). pp. 739-750. https://doi.org/10.1016/B978-0-12-813351-4.00042-0

[4] S.R.R. Reddy, P. Bala Anki Reddy, and A.M. Rashad, "Activation Energy Impact on Chemically Reacting Eyring–Powell Nanofluid Flow Over a Stretching Cylinder," Arab. J. Sci. Eng. **45**(7), 5227–5242 (2020). https://doi.org/10.1007/s13369-020-04379-9

[5] M. Gupta, V. Singh, R. Kumar, and Z. Said, "A review on thermophysical properties of nanofluids and heat transfer applications," Renewable and Sustainable Energy Reviews, **72**, 638-670 (2017). https://doi.org/10.1016/j.rser.2017.02.073
[6] B. Mehta, D. Subhedar, H. Panchal, and Z. Said, "Synthesis, stability, thermophysical properties and heat transfer applications of nanofluid – a review," J. Mol. Liq. **364**, 120034 (2022). https://doi.org/10.1016/J.MOLLIQ.2022.120034
[7] S.U.S. Choi, and J.A. Eastman, "Enhancing Thermal Conductivity of Fluid with Nanoparticles," ASME Fluids Engineering Division, Scientific Research Publishing," **231**, 99-105 (1995). https://ecotert.com/pdf/196525_From_unt-edu.pdf
[8] S. Jakeer, and P.B.A. Reddy, "Entropy generation on the variable magnetic field and magnetohydrodynamic stagnation point flow of Eyring – Powell hybrid dusty nanofluid: Solar thermal application," Proc. Inst. Mech. Eng. Part C J. Mech. Eng. Sci., **236**(13), (2022). https://doi.org/10.1177/09544062211072457
[9] N.S.M. Hanafi, W.A.W. Ghopa, R. Zulkifli, S. Abdullah, Z. Harun, and M.R.A. Mansor, "Numerical simulation on the effectiveness of hybrid nanofluid in jet impingement cooling application," Energy Reports, **8**, 764–775 (2022). https://doi.org/10.1016/J.EGYR.2022.07.096.
[10] Azmi, et al. "A review on thermo-physical properties and heat transfer applications of single and hybrid metal oxide nanofluids," Journal of Mechanical Engineering and Sciences, **13**(2), 5182-5211 (2019). https://doi.org/10.15282/JMES.13.2.2019.28.0425
[11] S. Arulmozhi, K. Sukkiramathi, S.S. Santra, R. Edwan, U. Fernandez-Gamiz, and S. Noeiaghdam, "Heat and mass transfer analysis of radiative and chemical reactive effects on MHD nanofluid over an infinite moving vertical plate," Results Eng. **14**, 100394 (2022). https://doi.org/10.1016/J.RINENG.2022.100394
[12] S.R.R. Reddy, and P.B. Anki Reddy, "Thermal radiation effect on unsteady three-dimensional MHD flow of micropolar fluid over a horizontal surface of a parabola of revolution," Propuls. Power Res. **11**(1), 129–142 (2022). https://doi.org/10.1016/J.JPPR.2022.01.001
[13] S. Jakeer, and B.A.R. Polu, "Homotopy perturbation method solution of magneto-polymer nanofluid containing gyrotactic microorganisms over the permeable sheet with Cattaneo–Christov heat and mass flux model," Proc. Inst. Mech. Eng. Part E J. Process Mech. Eng. **236**(2), 525–534 (2022). https://doi.org/10.1177/09544089211048993
[14] S. Jakeer, and P.B.A. Reddy, "Entropy generation on EMHD stagnation point flow of hybrid nanofluid over a stretching sheet: Homotopy perturbation solution," Phys. Scr. **95**(12), 125203 (2020). https://doi.org/10.1088/1402-4896/abc03c
[15] X. Zhang, Y. Chen, and J. Hu, "Recent advances in the development of aerospace materials," Prog. Aerosp. Sci. **97**, 22–34 (2018). https://doi.org/10.1016/J.PAEROSCI.2018.01.001
[16] H. Xia, P.G. Tucker, and W.N. Dawes, "Level sets for CFD in aerospace engineering," Prog. Aerosp. Sci. **46**(7), 274–283 (2010). https://doi.org/10.1016/J.PAEROSCI.2010.03.001
[17] M. Ramzan, F. Ali, N. Akkurt, A. Saeed, P. Kumam, and A. M. Galal, "Computational assesment of Carreau ternary hybrid nanofluid influenced by MHD flow for entropy generation," J. Magn. Magn. Mater. **567**, 170353 (2023). https://doi.org/10.1016/j.jmmm.2023.170353
[18] G. Ramasekhar, and P.B.A. Reddy, "Entropy generation on EMHD Darcy-Forchheimer flow of Carreau hybrid nano fluid over a permeable rotating disk with radiation and heat generation : Homotopy perturbation solution," Proc. Inst. Mech. Eng. Part E: J. Process Mech. Eng. **237**(4), 1179-1191 (2023). https://doi.org/10.1177/09544089221116575
[19] A. Divya, and P.B.A. Reddy, "Aerospace aspects of electromagnetohydrodynamic dusty fl ow of hybrid nano fl uid with entropy generation over a rotating disk," Proc. Inst. Mech. Eng. Part E: J. Process Mech. Eng. **237**(2), 196-206 (2023). https://doi.org/10.1177/09544089221102417

РОЗШИРЕНИЙ АНАЛІЗ ТЕПЛООБМІНУ МГД-ГІБРИДНОГО ПОТОКУ НАНОРІДИНИ НАД ПОРИСТОЮ ПОВЕРХНЕЮ, ЩО РОЗТЯГУЄТЬСЯ: ЗАСТОСУВАННЯ ДЛЯ АЕРОКОСМІЧНИХ ХАРАКТЕРИСТИК

Р. Чандра Секар Редді, Гунісетті Рамасекар
Факультет математики, Меморіальний коледж інженерії та технологій імені Раджива Ганді (автономний), Nandyal 518501, Андхра-Прадеш, Індія

Розвиток авіатехніки поставив перед виробниками нові критерії та проблеми для функціонування їхніх пристроїв. Важливо, щоб для гарантування безпечної роботи аерокосмічного обладнання було якнайшвидше визначено механізми відмови та покращено експлуатаційну довговічність критичних структурних компонентів. У сучасності були розроблені нові авіаційні матеріали. В авіаційних двигунах моторне масло змащує, охолоджує, промиває, захищає від іржі, знижує шум і прискорює. Метою даної роботи є мінімізація витрат за рахунок продовження терміну експлуатації компонентів літака (механічних і моторних частин) і збільшення запасу палива і дальності польоту. Виходячи з важливості натхнення щодо магнітогідродинамічного потоку гібридної нанофлюїду оксиду алюмінію та кобальту над поверхнею, що розтягується (SS) і існуванні пористого середовища, досліджено теплове випромінювання. У цій моделі ми використовували моторне масло, змішане з оксидом алюмінію та наночастинками кобальту. Використовуючи відповідні змінні самоподібності, PDE перетворюється в ODE. Після цього безрозмірні рівняння розв'язуються за допомогою схеми Maple, вбудованої в схему BVP Midrich. Графіки та таблиці пояснюють, як робочі фактори впливають на ефективність потоку рідини. Порівняно з нанофлюїдами гібридні нанофлюїди мають кращу швидкість теплопередачі.

Ключові слова: *схема BVP Midrich; МГД; теплове випромінювання; пористе середовище; гібридний нанофлюїд*